6

Ti:sapphire: Material, Lasers and Amplifiers

Peter F. Moulton, Alan R. Fry, and Peter Fendel

CONTENTS

6.1 Introduction

The Ti:Al_2O_3 (Ti:sapphire) laser has several ancestors, including the first laser [1], based on the crystal ruby, formally Cr^{3+} ions doped into sapphire (Al_2O_3). Ti:sapphire employs the same robust host crystal as in ruby, which is crucial for the ruby laser to operate under the intense optical pumping from flashlamps, required by the three-level nature of the ruby laser transition. Another class of ancestors were the first broadly tunable solid-state lasers, based on divalent transition-metal ions, such as Ni^{2+} and Co^{2+}, doped into mainly fluoride host crystals, such as MgF_2 [2–5]. While these types of lasers could be tuned over an impressive range of wavelengths (1600–2500 nm in the case of Co:MgF_2 [6]), the low gain and the general need to operate under cryogenic cooling were drawbacks that limited their utility. Finally, another Cr^{3+}-doped crystal, alexandrite ($BeAl_2O_4$), developed in the late 1970s [7,8] showed that tunable solid-state lasers could be made with robust host crystals and operate at room temperature. Later variations of the alexandrite laser, providing broader tuning ranges, included Cr^{3+}-doped fluoride materials [9,10], such as $LiCaAlF_6$ (LiCAF) and $LiSrAlF_6$ (LiSAF).

Presently, the Ti:sapphire laser has become the most widely employed tunable and ultrafast-pulse solid-state laser, and in the following brief review of solid-state laser fundamentals, we explain how its unique set of properties have enabled its widespread use.

6.2 Laser Material Properties

The unique combination of good spectroscopic and material properties is the major reason that Ti:sapphire became and still remains a widely used crystal for tunable laser systems.

Table 6.1 lists the room-temperature (unless noted) spectroscopic properties of several common solid-state laser materials. Ti:sapphire emerges as having similar cross sections and saturation fluences to Nd:YAG ($Y_3Al_5O_{12}$), one of the most widely used conventional (i.e. non tunable) solid-state materials. It also has the largest gain linewidth of all the materials shown,

TABLE 6.1

Spectroscopic Properties of Selected Solid-State Laser Materials at 300 K, Unless Indicated

Material	Peak Wavelength (nm)	Storage Time (ms)	Cross Section at Peak (cm^2)	Gain Linewidth (nm)	Saturation fluence ($J\ cm^{-2}$)
Nd:YAG	1064	0.24	2.8×10^{-19}	0.6	0.66
Yb:CaF_2	1030	2.4	3.0×10^{-21}	50	64
Co:MgF_2 (77 K)	1900	1.4	1.5×10^{-21}	600 (50 THz)	68
Cr:$BeAl_2O_4$	755	0.26	7×10^{-21}	55 (29 THz)	37
Cr:LiSAF	850	0.067	5.0×10^{-21}	190 (85 THz)	4.7
Ti:Al_2O_3	800	0.0032	2.5×10^{-19}	225 (100 THz)	1.0

supporting generation and amplification of pulses as short as 5 and 20 fs, respectively. A few the materials also have large linewidths but, in addition, high saturation fluences, limiting their use in pulse amplifiers.

Table 6.2 is another comparison table showing important thermo-optical and thermo-mechanical properties of some of the solid-state laser materials listed in Table 6.1. For non-isotropic materials, the values given represent those for the most favorable orientation and polarization.

A comparison of sapphire with the other materials points out the advantage of the crystal in high-power operation, as it has the highest thermal conductivity (with some variations in published data, as shown) and the highest thermal shock parameter. All of the properties in Table 6.2 for sapphire vary favorably at lower temperatures, as we discuss in more detail later in this chapter. The LiSAF material, which otherwise has excellent spectroscopic parameters, has limits to high-power operation, primarily from a low thermal conductivity.

Figure 6.1 shows the Ti:sapphire absorption (gray) and emission (black) cross sections as a function of wavelength. The solid lines are older line shape data [17] corrected for an

TABLE 6.2

Physical Properties of Selected Solid-State Laser Materials

Material	κ ($W\ m^{-1}\,°C^{-1}$) 300 K	κ ($W/m^{-1}\,°C^{-1}$) 100 K	α ($10^{-6}\,°C^{-1}$)	dn/dt ($10^{-6}\,°C^{-1}$)	E (GPa)	RT (W/m)	Refs.
YAG	10	58	6.7	8.9	282	1100	[11–13]
MgF_2	21	100	15	2.0	138	1300	[11,12]
$BeAl_2O_4$	23		4.4 (a) 6.8 (b) 6.9 (c)	9.4 (a) 8.3 (b)	446	2350	[12,13]
LiSAF	3.1		–8.1 (c) 26 (a)	–4.5 (n_o) –9.1 (n_e)	109	84 (a) 160 (c)	[14,15]
Al_2O_3	28–42	380	6.7 (‖ to c)	12.8 (‖ to c)	405	3400	[11,12,16]

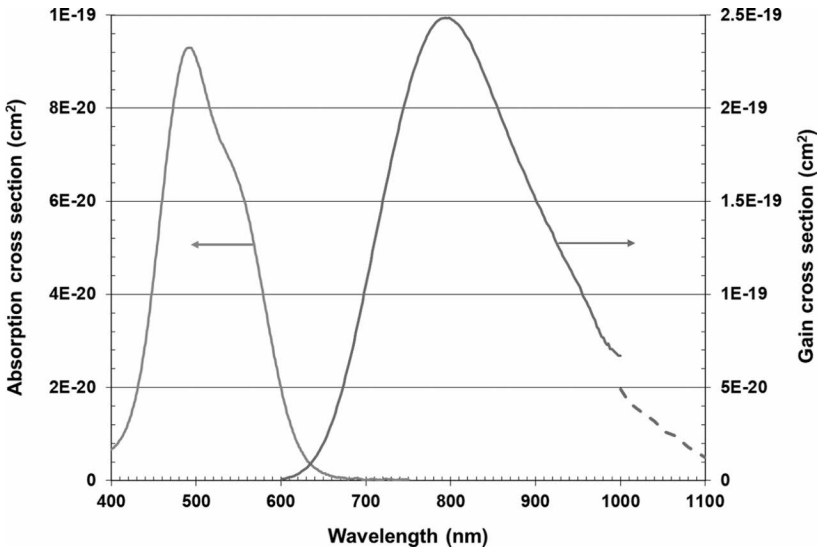

FIGURE 6.1 Data on Ti:sapphire absorption and gain cross sections as a function of wavelength, for π-polarized light.

absorption cross-section scale (left axis) derived by a newer, more accurate analysis [18], while the gain cross-section scale (right axis) reflects the consensus of several measurements [19–21]. Gain data at wavelengths longer than 1000 nm from [17] have been omitted due to the increasing level of noise from the detector used in the original measurements. However, included in the plot (dashed lines) are long-wavelength gain cross-section data derived from direct gain measurements [20].

The absorption band in Figure 6.1 shows that optical pumping of Ti:sapphire can be accomplished through the use of a variety of different lasers. Early cw operation with pumping by argon-ion gas lasers (488–515 nm) has been superseded by use of frequency doubled, Nd-doped and Yb-doped solid-state lasers, or by optically pumped semiconductor lasers (OPSL). Pulsed pumps include the same solid-state lasers operating in the nanosecond-pulse regime, and, for very high-energy systems, doubled Nd:glass lasers. Recently, GaN-based diode lasers have become available with sufficient power and brightness to pump Ti:sapphire lasers, and future diode developments may provide a path to more efficient, compact and inexpensive systems.

6.2.1 Material Physics, Properties and Growth

The Ti:sapphire laser transition occurs between energy levels associated with the single 3d-electron in the outer shell of the Ti^{3+} ion. The normally five-fold degenerate, free-space 3d-electronic state is split when the ion sits in the sapphire crystal at a site normally occupied by an Al^{3+} ion. That field at the site is nearly cubic in symmetry, with a strong trigonal component. The lowest-energy state ($^2T_2$) is a three-fold nearly degenerate level and splits slightly into two main levels by the trigonal field, with the lower level splitting further by a spin-orbit interaction [22–24]. The two-fold-degenerate upper laser level (^2E) interacts with the host crystal through the Jahn-Teller interaction to split into two spatially disjoint, but equal-energy states.

We have listed some of the properties of the host crystal, sapphire, in Table 6.2, and there is ample literature on other properties, as the material finds widespread use, ranging from substrates for semiconductor devices, protective covers on cellphone cameras to windows on military equipment such as tanks. It is produced in yearly quantities of several hundred tons. In terms of hardness, sapphire is below only diamond and silicon carbide. The crystal structure is of the trigonal space group R$\underline{3}$c, and is uniaxial, with a slight birefringence of about 0.008, and an index of about 1.76–1.77 [25]. Optical properties are given with respect to polarization either parallel to the crystal c-axis (pi-polarized) or perpendicular (sigma-polarized). In Ti:sapphire, the absorption and emission properties are strongly polarized in favor of pi-polarized light for both absorption and emission [15].

From the standpoint of laser design, one important practical material property is the absorption coefficient (typically in cm^{-1}) of the pump-band light. This is proportional to the Ti^{3+} concentration in the crystal. Unfortunately, there are several different ways to specify this, including the actual ion density (ions/cm^3), Ti^{3+} doping in molecular % or weight %, Ti_2O_3 doping in molecular % or weight %, and sometimes just a % doping, with no indication of what the % signifies. As an example of one relationship, if α_{490} is the absorption at 490 nm for π-polarized light, then

$$\text{Weight\% } Ti_2O_3 = (0.032 \pm 0.003)\alpha_{490}, \tag{6.1}$$

where the presumption is that all of the Ti ions are in the 3+ state [18].

In specifying material, the safest approach is to specify the desired pi-polarized absorption coefficient. In some cases, vendors may quote absorption at 514 nm (α_{514}), a convention from the period when argon-ion lasers were widely used as pump sources, and the absorption there is about 0.875 of the value at 490 nm.

In terms of material growth, commercial materials have been prepared using variations in the Czochralski crystal-pulling-from-the-melt technique, with the use of post-growth annealing to improve the FOM [26]. Another widely utilized approach is the Heat-Exchanger Method (HEM) [27], which has been used to grow very large-size materials needed for high-energy laser systems.

6.3 Laser Systems

After reviewing some basic material properties of Ti:sapphire in the previous section, the rest of this chapter will focus on the use of Ti:sapphire as a gain material in laser oscillators and amplifiers. Because of its favorable thermal and spectroscopic properties, Ti:sapphire has been used in countless different laser and amplifier configurations. Only the most common are described below, and references are given for those who want to get a more comprehensive overview.

6.3.1 Oscillators

6.3.1.1 Tunable cw Lasers

Under cw pumping conditions, and with no loss due to excited-state absorption of the pump or other complications, the cw gain per unit length, g_0, of a laser material with uniform pumping can be expressed as follows:

$$g_0 \propto \alpha\ W_p \lambda_p^4 / n^4 \Delta\lambda, \tag{6.2}$$

where W_p is the pump rate in excitations/($cm^3 s^{-1}$), λ_p is the peak gain wavelength, and $\Delta\lambda$ is the gain linewidth of the transition, given in units of wavelength. For a broad-linewidth material such as Ti:sapphire, achieving sufficient gain for laser action requires relatively high optical pumping rates. This leads to the use of cw lasers as pump sources, focused to high intensities in the Ti:sapphire laser medium.

For laser-pumped materials pumped along the direction of the laser beam (longitudinal pumping), the pump power (P_{th}) required to reach the threshold of laser action can be approximated by the following equation [28]:

$$P_{th} = \eta_c \frac{\pi h \nu_p}{4\sigma_p \tau} (T + L_{cav} + L_{XTL})\left(w_0^2 + w_p^2\right)\left[1 - \exp(-\alpha l)\right]^{-1}, \tag{6.3}$$

where η_c is the coupling efficiency of the pump beam into the laser crystal, which accounts for losses in the optical elements between the pump laser and the inside of the laser material; h is Planck's constant; ν_p is the frequency of the pump laser; σ_p and τ are the peak gain cross section and upper-state lifetimes discussed above, respectively; T is the transmission of the (assumed single) output-coupling (OC) mirror; L_{cav} is the total loss in the optical cavity from other than the output coupler and laser crystal; L_{XTL} is the loss in the crystal; w_0 and w_p are the mode radii of the laser and pump beams in the crystal, respectively; α is the absorption coefficient in the crystal for pump light; and l is the length of the crystal. The equation assumes the use of a standing-wave resonator, where the losses are calculated per round-trip (i.e. two-pass) in the cavity and crystal. For a ring-cavity system, the factor 4 in the equation must be changed to 2, since the laser beam is only amplified in one pass through the crystal, but this is mitigated by the reduced losses due to single passes in the cavity and crystal.

The assumption in Equation (6.3) is that the pump and laser beams are Gaussian in cross section and the mode sizes are uniform inside the crystal, i.e. the confocal lengths of the pump and laser beams are longer than the crystal, or the inverse of α, when the latter is large compared to the crystal length. Good design practice is to limit the length of the crystal such that αl is in the range of 2–3, as longer crystals provide marginally lower thresholds and can increase the threshold due to crystal loss. When the assumption of uniform pump and laser beam sizes in the crystal is not appropriate, the threshold increases and calculations become more complex [29]. The use of a single-mode pump laser leads to the lowest thresholds, since it allows smaller radii pump beams that still maintain a uniform beam size in the crystal.

For cw Ti:sapphire lasers, typical pump-beam mode radii are in the 25–50 μm region, to obtain thresholds on the order of a Watt with output couplers in the 2%–10% transmission range. This requires optical resonators designed to match the laser cavity mode size to this relatively small beam. The design is complicated by the desire to operate the gain medium at Brewster's angle to the resonator axis, minimize reflection losses over a wide wavelength range and eliminate the need for anti-reflection coatings that can suffer optical damage. The presence of a Brewster's angle element adds astigmatism (different optical paths for beam transverse axes in the Brewster plane of incidence and perpendicular to it) that can produce an elliptical cross section, rather than round output beam for resonators with a small mode size.

With the use of a Brewster's angle crystal, Equation (6.3) must be multiplied by n, the Ti:sapphire index of refraction (about 1.76), since the pump and laser beams inside the crystal are elongated in one dimension by this factor, thus reducing the pump intensity and gain by the same amount.

Figure 6.2 shows the typical cavity designs used for cw-pumped Ti:sapphire lasers. Both standing-wave and ring-cavity designs are illustrated. The standing-wave design is the so-called "W" configuration, with an alternative, the "Z" arrangement, achieved by rotating one of curved mirrors about the axis established by the beam in the crystal. The designs provide tight focusing for the cavity mode in the laser crystal and also, through the use of off-axis mirrors, correction for the astigmatism created by Brewster's angle laser crystal in between the two focusing mirrors. This approach was first developed for cw lasers based in liquid dyes [30] with a three-mirror design, subsequently improved to a four-mirror design that provided a single focal spot in the laser medium [31]. The four-mirror design has been readily adapted for cw Ti:sapphire lasers. Cavity designers often employ the ABCD matrix approach [32] to work out the correct choice of mirror curvatures and spacings, with the addition of the ABCD matrix for off-axis curved mirrors [33]. The technique becomes increasingly necessary for even more complex designs than in Figure 6.2, involving other curved mirrors to produce added intracavity small spot sizes for use with nonlinear crystals or high-speed acousto-optic modulators. The designs also provide cavity beams between the focusing mirrors and HR or OC mirrors that have relatively large, nearly uniform mode sizes. The cavity parameters are relatively insensitive to the exact optical path for the beams, allowing insertion of Brewster's angle optics with minimal addition of astigmatism to the cavity mode. The ring-cavity design facilitates single-frequency operation through elimination of spectral hole-burning (for more details, see Refs. [34–38]).

With the desire to use a low-transmission output coupler to keep the threshold low, it becomes important that other optics in the cavity also have low losses. One key intracavity optic for Ti:sapphire lasers is the tuning element. While Brewster's angle prisms are one option, birefringent filters (BRFs), another technology with origins from cw dye lasers [39], are more common. The filters are based on uniaxial birefringent crystals placed at Brewster's angle to the resonator beam (Figure 6.2) to provide a low-loss tuning element. BRFs can be viewed as a variation of the etalon concept. When ab interference between the transmitted and reflected beams creates a wavelength-varying transmission in an etalon, a BRF operates on the interference between the two linearly and orthogonally polarized beams that represent the general state of polarization

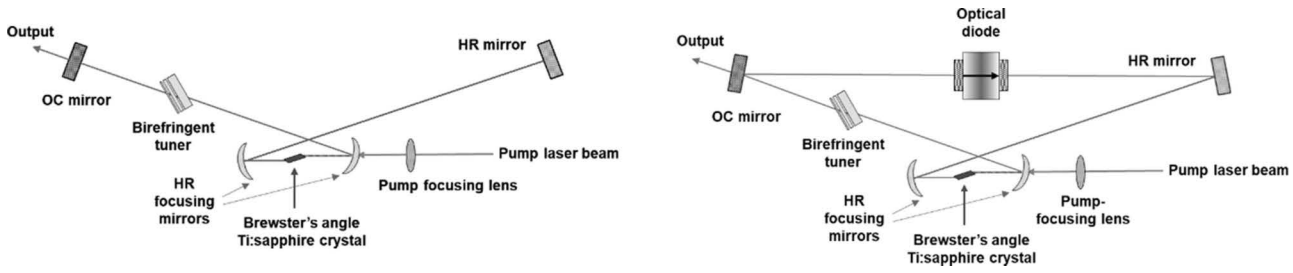

FIGURE 6.2 Optical schematics of cw Ti:sapphire lasers, standing-wave (left) and ring-cavity (right) designs.

inside a birefringent crystal. With a given thickness, orientation and birefringence for single BRF crystal, a cavity optical beam with incoming linear polarization will generally exit the BRF with elliptical polarization, due to the optical phase difference between the two orthogonally polarized beams. Only when the wavelength of the beam produces a phase difference that is an integer multiple of π (a resonance for the BRF), the beam polarization state will remain linear and not suffer loss at the exiting Brewster surface. Modern designs [40] use off-axis plates to enable broad tuning ranges. Details of BRF designs can be found in Refs. [41–46].

Figure 6.3 shows the tuning curve for a commercial cw Ti:sapphire laser, showing coverage from 670 to 1100 nm, possible through the use of three different sets of cavity mirrors. The challenge is clear to designing a BRF that covers this range and provides enough spectral rejection to permit operation at either extreme of the gain region.

The earliest cw Ti:sapphire lasers employed argon-ion lasers as pumps, but they have been replaced by cw, frequency-doubled solid-state lasers, typically based on diode-pumped, Nd:YVO_4 lasers and doubled Yb:fiber lasers, and frequency-doubled, OPSLs. Recently, InGaN-based semiconductor lasers have become available with sufficient brightness for pumping cw lasers [48–52] and at present are capable of producing Ti:sapphire powers around 0.5 W. Published work indicates that use of 450 nm-region diodes can induce extra loss in the Ti:sapphire crystal [48] and yields lower efficiency than expected [52]. Thus, diodes at longer wavelengths are more desirable. The reason for this effect has been recently identified, and optimal diode wavelengths for pumping are at 490 nm and longer [53,54].

6.3.1.2 Short-Pulse Laser

The relation between pulse duration $\Delta\tau$ and the bandwidth $\Delta\omega$ required to support such pulse is described through the time-bandwidth product: $\Delta\omega \times \Delta\tau = \text{const}$ [55]. One of the key properties of Ti:sapphire is its broad gain spectrum, which covers several hundred nanometers, thus supporting extremely short, on the order of 5 fs, laser pulses.

In general, a laser cavity only supports a discrete spectrum. Each longitudinal cavity mode needs to satisfy the geometrical condition $n\lambda/2 = L$ (n being an integer and L the optical path length). The mode spacing is given by the inverse of the cavity round-trip time and lies typically based on geometric considerations in between 10 MHz and 1 GHz, which corresponds to a cavity length of approximately 15 m and 15 cm, respectively, for a linear cavity.

Combining this with the requirements imposed by the time-bandwidth product a short-pulse laser cavity needs to lase on a large number (>10^4) of modes to cover the required bandwidth for an fs pulse. Lasing on many modes, however, is necessary but not sufficient to generate short pulses from a laser cavity.

It is well known that light with different frequencies propagates with different phase velocities through space except when in vacuum, a phenomenon called dispersion. As a consequence, unless dispersion is managed properly (see below), no short-pulse formation in a laser cavity is possible as different parts of the spectrum (different modes) would have slightly different round-trip times leading to the pulse spreading out in time. But even if the dispersion is managed properly in a laser cavity, it is not guaranteed for the laser to produce short pulses. In order to do that, all longitudinal modes in the cavity need to be forced into "lock-step" with each other so that they add up coherently and produce a single short pulse.

Various methods are used in scientific and commercial lasers to lock the cavity modes together. Most techniques rely on a cavity design which favors high peak power operation over steady-state cw operation by either increasing the gain or reducing the interactivity losses when the laser produces ultrashort pulses. For Ti:sapphire lasers, the most common mode-locking mechanism is the Kerr Lens mode locking [56,57], though other techniques like using a saturable absorber [58] also exist. A comprehensive discussion of mode locking can be found in Refs. [59–63].

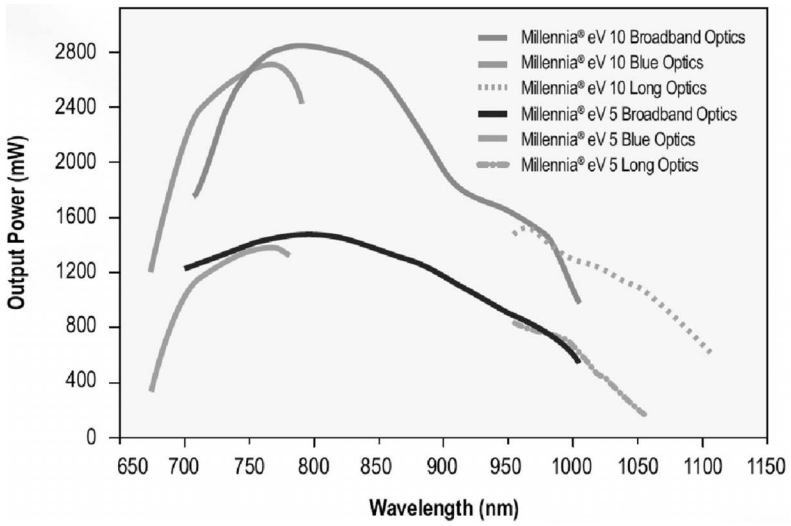

FIGURE 6.3 Tuning curve for commercial Ti:sapphire laser (Spectra-Physics 3900S) with three different optics sets (Broadband, Blue and Long) and with 5 W, and 10 W, 532 nm pump powers (Millenia eV 5 and 10) [47].

6.3.1.3 Dispersion Management

Many techniques for managing the dispersion in Ti:sapphire laser resonators have been developed over the past two decades. Unfortunately in the operating wavelength region of a Ti:sapphire laser, no negative dispersion materials, i.e. materials in which blue light travels faster than red light, are readily available. The three most common ways to introduce negative dispersion in the near IR are the Gires–Tournois interferometers [64], a combination of 2 or 4 prisms [65,66] and chirped mirrors [67].

Prisms are an easy and versatile way to control dispersion in a laser cavity. Two basic geometries employing either 2 or 4 prisms are possible, and both have been used in commercial laser systems. A typical 2-prism cavity is shown in Figure 6.4. The idea behind any dispersion management tool is to introduce a wavelength-dependent optical path length or phase difference. In case of prisms, each wavelength travels on a different trajectory through the prism assembly accumulating slightly different phase along the way. The prism material, degree of prism insertion and the distance between the two prisms determine the amount of dispersion the assembly introduces.

A detailed derivation of the dispersion of such prism assemblies introduce can be found [65]. The GDD is approximated by

$$\mathrm{GDD}(\lambda) \approx -4\, d\, \frac{\lambda_0^3}{2\pi c^2}\left(\frac{dn}{d\lambda}\Big|_{\lambda_0}\right)^2 + D\frac{\lambda_0^3}{2\pi c^2}\frac{d^2 n}{d\lambda^2}\Big|_{\lambda_0}$$

with d being the separation between the two prisms and D being the insertion. In order to avoid the Fresnel reflection losses, the prism should be used under Brewster's angle [68]. The apex angle α itself should follow this equation to minimize losses also on the second prism surface:

$$\alpha = 180° - 2\theta_B$$

θ_B being the Brewster angle for the material the prism is made from.

Prisms work well for lasers with pulse durations above 12 fs. However, the dispersion manipulation prisms can provide is insufficient once the simultaneous lasing bandwidth approaches 100 nm. In this case, not only second and third orders but higher orders of dispersion terms also need to be managed [69,70]. A state-of-the-art solution is a chirped mirror [67]. A chirped mirror is a dielectric mirror which in addition to being a high reflector also alters the spectral phase of the reflected light in a controlled manner. The phase response or dispersion of a chirped mirror is given by the interference inside of the layer stack and not – to first order – by the material of the layer stack itself. This allows laser designers a lot of freedom in shaping the dispersion of the laser cavity and to carefully control higher-order dispersion terms which is essential for sub 10 fs laser operation.

The basic and greatly simplified operating principle of a chirped mirror relies on the principle that different colors experience different penetration depths into the thin film layer stack (see Figure 6.5). For negatively chirped mirrors, short-wavelength light is reflected on top of the mirror, while the long part of the spectrum penetrates deep into the layer stack accumulating a phase delay compared to the blue part of the spectrum. The dispersion of such a mirror is opposite to material dispersion in the near IR and can hence be used for dispersion management.

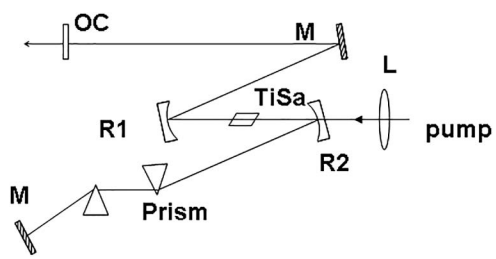

FIGURE 6.4 Typical cavity layout for a Ti:sapphire laser using prisms for dispersion compensation.

6.3.1.4 Frequency Combs and Carrier Envelope Phase

The concept of frequency combs or carrier envelope phase is not limited to Ti:sapphire lasers but applies to all mode locked lasers. Ti:sapphire lasers, however, were the first lasers in which a fully stabilized, self-referenced comb was demonstrated [71,72].

A detailed description about frequency combs can be found in Refs. [73–75]. The seminal work on this topic by Hall and Hänsch in the late 1990s is of long reaching significance for the ultrafast as well as the frequency metrology community enabling, e.g., optical clocks [76] or the generation of attosecond pulses [77].

The most difficult part in realizing a frequency comb was to measure and control the phase and the phase slip between the carrier wave and the envelope function, the so-called carrier envelope phase (CEP) or the carrier envelope offset frequency f_{ceo} [78,79] (see Figure 6.6). The shift in CEP from pulse to pulse originates from the fact that the carrier propagates with its phase velocity, i.e., speed of light, while the amplitude function propagates only with the group velocity.

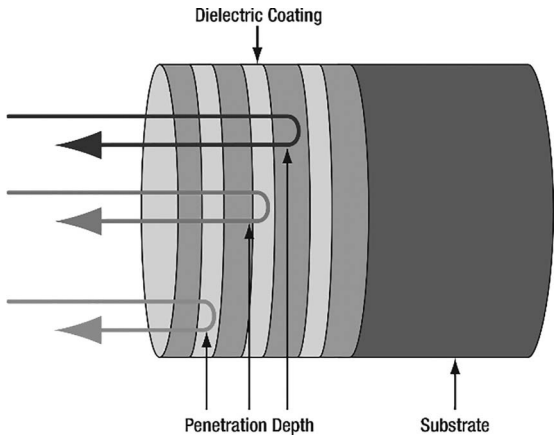

FIGURE 6.5 In a chirped mirror, different wavelength experience diffrenet penetration depths into the dielectric coating and hence chirped mirrors introduce dispersion.

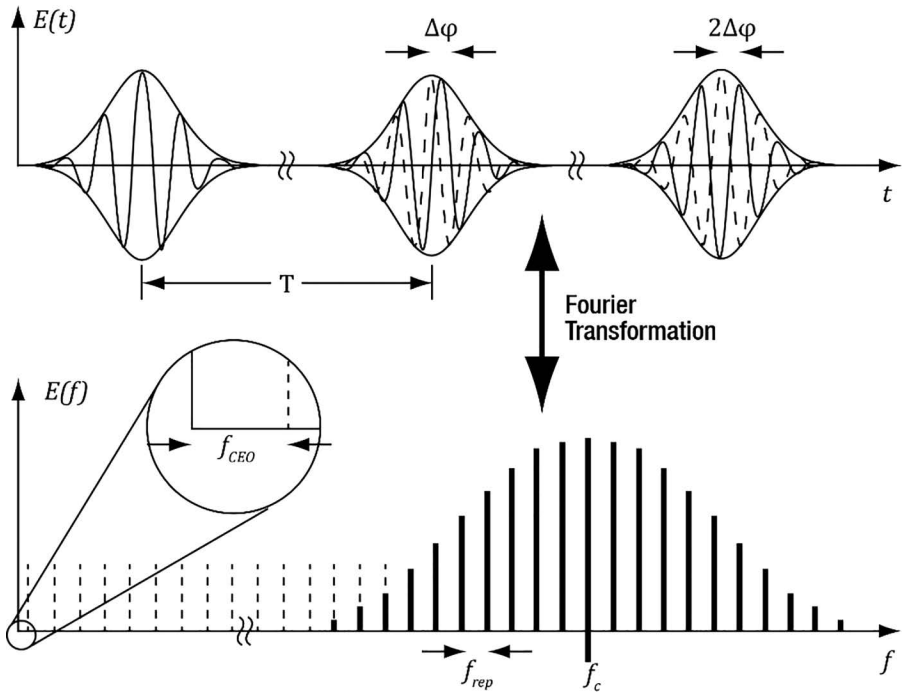

FIGURE 6.6 An fs pulse train and a frequency comb are linked through Fourier transformation. The mode spacing is given by the repetition rate [74].

For particular applications like high harmonic or attosecond pulse generation, it is vital that one generate femtosecond pulses with a specific and constant carrier envelope offset phase [77].

6.3.2 Amplifiers

Femtosecond pulse oscillators typically operate with pulse energies in the range of a few nJ up to hundreds of nJ in gain-switched Ti:sapphire oscillators. A number of schemes have been developed to increase the energy of Ti:sapphire systems, spanning several orders of magnitude in repetition rate and pulse energy, ranging from hundreds of kHz at μJ energy to tens of J in single-shot configurations. The most common commercial Ti:sapphire systems are configured in a well-established and widely adopted middle range of a few to tens of mJ operating at a few kHz repetition rate, e.g. 1 kHz, 5 mJ, 5 W average power. The pulse duration of a Ti:sapphire amplifier can also span several orders of magnitude from <10 fs to >1 ps, with the most common commercial systems operating in the range of 30–50 fs FWHM.

In most applications of amplified ultrafast laser pulses, the key parameter is the pulse intensity rather than the pulse energy or average power. This requires that amplified beams have a "clean" spatial profile that can be focused to the desired spot size to achieve the necessary intensity. In some cases, particularly in very high-intensity applications, it is also necessary to have a "clean" temporal profile, free of pre- and post-pulses.

Nearly every Ti:sapphire amplifier utilizes the technique of chirped pulse amplification (CPA), in which the seed laser pulse from a Ti:sapphire oscillator is temporally stretched by several orders of magnitude in a dispersive optical system, amplified and then recompressed in another dispersive optical system. The chirped-pulse amplification technique [80] was developed to reduce the peak power in high-energy Nd:glass amplifiers [81] and was quickly adapted to Ti:sapphire systems [82].

6.3.2.1 Amplifier Design

The laser designer will optimize the energy of a Ti:sapphire laser amplifier by achieving the highest possible gain for a given pump energy without introducing temporal or spatial distortions to the amplified pulse. The amplified pulse should reach the saturation fluence for the highest efficiency and the highest shot-to-shot energy stability, as well as to ensure that the dispersion associated with the amplification is linear across the temporally chirped pulse to achieve consistent recompression. Over-saturation of the pulse can result in changes in the pulse intensity profile, specifically higher amplification of the temporally leading edge of the pulse, and in a CPA configuration, this effect will also result in a spectral reshaping of the amplified pulse due to the longer wavelengths temporally preceding the shorter wavelengths.

Ti:sapphire amplifier designs must also optimize the overall dispersion of the CPA system including the total group velocity dispersion (GVD) of the optical elements in the amplifier. High GVD due to a large number of optical elements is significantly more challenging for very short (<30 fs) laser pulses with correspondingly large (>30 nm) bandwidths, and many amplifier designs are fine-tuned in terms of the selection of the type and thickness of materials used in the amplifier stages.

Gain narrowing is an important consideration in amplifier design, but it is not commonly a significant problem for Ti:sapphire due to its extremely broad gain bandwidth. Again it is only in applications that require extremely broad

bandwidths (e.g. >100 nm for a <10 fs pulse), or in cases where it is desirable to shift the center wavelength of the output of the Ti:sapphire amplifier by many tens of nm away from the peak of the gain near 800 nm. It is more often the case that the bandwidth of the Ti:sapphire amplifier is limited by the spectral bandwidth of other elements of the Ti:sapphire amplifier, such as the reflectivity of the dielectric coatings of the mirrors.

A more detailed descriptions about the general architecture of CPA systems, e.g. strechter and compressor designs, can be found in Ref. [83].

6.3.2.2 Regenerative Amplifiers

The regenerative amplifier [84] (commonly abbreviated "regen") is the first most commonly used amplification stage in commercial Ti:sapphire systems. A typical Ti:sapphire regenerative amplifier configuration is shown in Figure 6.7. In this figure, the pump beam is shown in green, and the seed and amplified Ti:sapphire beams are shown in red. Two Pockels cells are used as electro-optical switches, and two polarizers are used: one to inject the seed beam and the other to eject the amplified beam after the last round-trip, both arranged for transmission in P-polarization. When the regen cavity is inactive, seed laser pulses are continuously injected into the regen cavity, reflecting in S-polarization off the input polarizer (P1) into the cavity. These pulses double-pass through the input Pockels cell (PC1) and quarter waveplate (QWP) for a net rotation of half-wave to P-polarization. The pulses then make a complete round-trip through the regen cavity, through the Ti:sapphire crystal, the output polarizer (P2), the output Pockels cell (PC2), and then back through the entire cavity. Upon making a second round-trip through the QWP, the pulse is again S-polarized and is rejected from the cavity from the input polarizer (P1). During amplification, the typical sequence of events follows: first, the Ti:sapphire crystal is pumped by a pulsed or CW pump source. When the Ti:sapphire is sufficiently pumped to achieve the necessary gain, the input Pockels cell (PC1) is activated to produce a quarter-wave rotation, so that in combination with the QWP, there is net-zero round-trip change in the polarization state of a P-polarized seed pulse making its return trip through the cavity (similarly, any subsequent seed pulses entering the cavity stay in their S-polarization state and are rejected from the input polarizer after a single half-round-trip). The selected, P-polarized seed pulse then makes multiple round-trips through the cavity, continuing to extract the stored energy in the Ti:sapphire crystal. When the maximum gain and saturation of the amplifier are achieved, the output Pockels cell (PC2) is activated a quarter-wave rotation so that when the amplified pulse makes a round-trip through this Pockels cell, the net half-wave rotation switches the pulse to S-polarization, and it is rejected from the cavity through the output Pockels cell (P2).

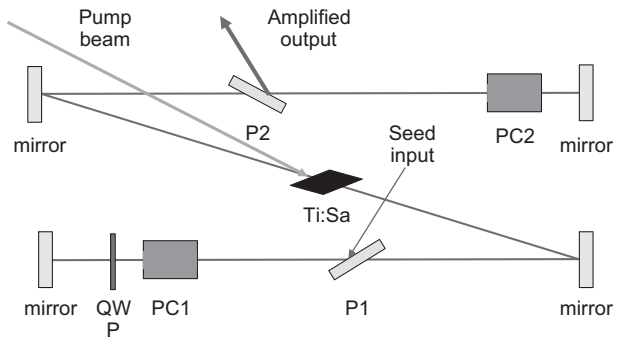

FIGURE 6.7 Schematic layout of a regenerative amplifier cavity.

To maximize efficiency in any regenerative amplifiers, it is necessary to use optical elements that have low losses for the amplified beam, e.g. high-reflectivity cavity mirrors, high-transmission Pockels cells, waveplate, and Ti:sapphire crystal. Polarizers must have high transmission in P-polarization and simultaneously high reflectivity in S-polarization. The coatings for the optics in Ti:sapphire regen amplifiers can be especially challenging due to the broad-bandwidth Ti:sapphire; these coatings must have correspondingly broad-bandwidth as well as relatively flat spectral phase characteristics. An additional requirement for these coatings is moderate to high damage threshold as the peak fluence and peak intensity the amplified pulses in the cavity can become quite high. In general, optical coatings with the broadest bandwidth and flattest spectral phase have lower damage threshold than coatings with narrower bandwidth, and it can be necessary to trade-off between these features and to consider cavity designs that increase the amplified spot size on critical optics.

Another practical consideration for the selection of components in Ti:sapphire regenerative amplifiers is the total chromatic dispersion and accumulated higher-order spectral phase from transmission through the intracavity components. Normally, the stretcher/compressor system is designed to accommodate this dispersion over some range of round-trips, and changes in the dispersion of a different number of round-trips can be compensated with a small adjustments, e.g. to the compressor grating separation and/or grating angle.

In a typical, commercial, 1 kHz Ti:sapphire regenerative amplifier pumped with 20 mJ of 527 nm light from a Q-switched, frequency-doubled Nd:YLF laser, a seed pulse of a few nanojoules energy is amplified to >5 mJ in ~15 round-trips, corresponding to a total net gain of ~10^6 and a net round-trip gain of ~3. For a seed pulse with a bandwidth of >50 nm, FWHM (Gaussian) gain narrowing from amplification and the transmission and reflection bandwidth of intracavity optics will typically reduce the spectral bandwidth to around 30 nm FWHM (Gaussian), corresponding to a transform-limited pulse duration of ~30 fs FWHM.

A broader spectrum and narrower pulse duration can be achieved by means of intra-cavity elements with specifically tailored spectral response to increase losses near the peak of the Ti:sapphire gain to effectively "flatten" the spectral reshaping from the gain narrowing; such systems can achieve ~20 fs, with singular demonstrations as low as 12 fs [85–87].

Similarly, Ti:sapphire regen amplifiers can be configured to operate with amplified pulses having a peak at nearly any wavelength within the broad gain bandwidth, albeit with narrower spectral bandwidth. Cavity optics coated to have high loss at the peak of the gain of Ti:sapphire (~800 nm) and high reflectivity at another wavelength range can produce, for

example, pulses centered at 760 nm [88] for the LCLS photoinjector, or at 1053 nm [20] for seeding a high-energy Nd:glass amplifier system.

6.3.2.3 Multipass and Multi-stage Amplifiers

In a multipass amplifier [89,90], a set of mirrors are arranged to provide multiple, slightly offset beam paths through the pumped region of the Ti:sapphire crystal in a fixed number of passes. This is a conceptually simple configuration with the advantage of having a smaller GVD compared to a regenerative amplifier, but can become difficult to align and optimize is the number of passes through the Ti:sapphire is high. Consequently, multipass amplifiers are better suited to systems requiring very high pulse energy in which the input pulse energy is already high relative to the saturation fluence of the amplifier, and saturation can be reached within 2–10 passes.

The most common commercial, few mJ Ti:sapphire laser systems are comprised of a single stage of amplification, either a regenerative amplifier or a multipass amplifier. Nearly, all higher-energy systems delivering 10 mJ or more are comprised of multiple stages of amplification, often with each stage having its own pump source, and operating at its own maximum rep-rate. A typical commercial configuration for a system generating pulses of 100 mJ energy would have an oscillator seeding a 1 kHz regenerative (or multipass) amplifier pumped by a q-switched, diode-pumped, frequency-doubled Nd:YLF laser to produce 5 mJ which would be picked down to a 10 Hz pulse train to seed a multipass amplifier pumped by a 10Hz q-switched, flashlamp-pumped, frequency-doubled Nd:YAG laser to produce 130 mJ before compression.

6.4 Exotica

6.4.1 Petawatt Systems

Scaling of CPA Ti:sapphire systems to very high peak powers, 1 PW (10^{15} W), and higher, has been accomplished, typically with compressed pulse energies of >30 J, and pulse widths on the order of 20–30 fs. The approach involves a series of amplifier stages, each pumped by higher-energy pumps. As the stages scale up in energy, they use larger-aperture beams and crystals to avoid optical damage to the laser medium and associated optics.

Early PW-class systems started with a Ti:sapphire femtosecond oscillator, typically followed by a Ti:sapphire-based regenerative amplifier, and then by staged amplifiers, with multipassing used to assure efficient extraction of pulse energy. For most scientific applications, it is very important to obtain a very high contrast (>10^{10}) between the main output pulse and any other pulse energy on either temporal side of that pulse. PW-class systems include a variety of techniques to improve pulse contrast. Some recent designs have employed optical parametric chirped pulse amplifiers (OPCPAs), which, under the right operating conditions [91], provide a unique combination of very high gain, broad gain bandwidth, and relatively low background pulse energy. Other techniques to improve pulse contrast include the addition of a cross-polarized wave (XPW) nonlinear element at some point in the amplifier chain [92]. The device operation is based on the use of third-order nonlinearity in a crystal, and hence is effective at suppressing low-energy content in the amplified pulse.

High-energy operation of Ti:sapphire brings challenges from the large-aperture crystals needed to avoid optical damage. They can lose energy stored from the pump laser through amplified spontaneous emission (ASE) along the transverse dimension of the laser crystal. Standard ASE-mitigation techniques include the use of absorbing media placed at the outer edge of the laser crystal. Another technique is to stagger the pump pulses in time to avoid too high a stored energy, and extract energy during the pumping process, a technique referred to as extraction during pumping (EDP) [93,94].

At the time of this writing, the field of PW-class Ti:sapphire lasers is dynamic, with new systems being developed and installed worldwide. One former (2017) peak-power record (5.4 PW) for any laser was set by a Ti:sapphire system [94], and in 2019, one of the 10-PW systems under construction [95–97] reached operational status at ELI-NP to set a new record.

A report from the U.S. National Academies of Sciences provides a more detailed technical discussion of PW-class Ti:sapphire lasers, with information on the status as of 2017 [98].

6.4.2 Cryogenically Cooled Systems

Ti:sapphire has unusually favorable properties regarding thermal effects, having a high thermal conductivity, which leads to lower thermal gradient in the crystal for a given level of power dissipation, and also a high stress-fracture limit. At high-enough powers, the material does exhibit optical distortion, mostly from the refractive index change. (Sapphire is naturally birefringent, and stress-induced birefringence in the material is small compared to the inherent birefringence, so losses in polarized resonators are not an issue. This is in comparison to isotropic materials such as YAG or glasses.) At sufficiently high powers, the refractive index distortion in Ti:sapphire can be enough to create unwanted changes in the cavity mode properties, in the case of oscillators, or the output-beam properties, in the case of amplifiers.

Cooling the Ti:sapphire crystal to cryogenic temperatures results in a dramatic change in the thermal, optical and mechanical properties that all relate to refractive-index distortion created by laser operation.

Table 6.3 compares important properties of sapphire at 300 and 100 K. Besides the dramatic increase in thermal conductivity, the change of refractive index with temperature undergoes a significant reduction, so that thermal gradients that do exist have a reduced effect on the refractive index. In addition, the major reduction in thermal expansion greatly reduces stresses in the material. This reduction also minimizes changes in the shape of the material surface, which can also modify its optical properties.

The major disadvantage with cooling is the reduced heat capacity. For a pulsed pump source, such as the ns-duration Q-switched laser pumps used for high-energy lasers, the initial temperature rise is much faster than the time it takes for heat to flow out of the pumped region and is thus mainly determined

TABLE 6.3

Sapphire Properties at 300 and 100 K [99]

Property	300 K	100 K
Thermal conductivity, κ (W cm^{-1} K^{-1})	0.33	10
Index change with temperature, dn/dT (K^{-1})	12.8×10^{-6}	1.9×10^{-6}
Thermal expansion coefficient, α (K^{-1})	5.0×10^{-6}	0.34×10^{-6}
Volumetric heat capacity (J K^{-1}cm^{-3})	3.1	0.25
Thermal diffusivity (cm^{2}s^{-1})	0.1	40

by the heat capacity of the material. At 100 K, the initial heat rise would be about ten times higher than at 300 K. This is mitigated by the reduction in index change this rise will create, as well as the reduced thermal expansion and hence stress. In addition, the very large increase in thermal diffusivity at 100 K means that the heat flows very quickly away from the pumped volume, so, except at very high pulse rates, or for large pump volumes, the material settles back to the overall heat rise set by the average heat dissipation. In one case, calculations showed that steady state would be reached in 30 μs at 100 K, but this number is highly dependent on the dimensions of pump and laser beams in the crystal [99].

Another important consideration for Ti:sapphire lasers is the rapid reduction in upper-state lifetime above 300 K. This results in additional heating in the material under pumping conditions, as the reduction is associated with non-radiative transitions from the upper to lower laser levels. This can lead to a "thermal runaway" as higher temperatures lead to higher non-radiative losses and hence even more heating. The use of cryogenic cooling assures that except for the most extreme conditions, thermal runaway will not be present in the laser system.

Cryogenic cooling has enabled power scaling of Ti:sapphire regenerative amplifiers used in moderate-energy ultrafast laser systems. Before compression, a 10 kHz-rate amplifier produced 40 W of average power with a 180 W-average-power pump laser, leading to 26 W average-power compressed pulses with 58 fs pulse width [100]. A cryo-cooled, higher rate (100 kHz) system has produced up to 4.8 W of power before compression through use of a 37 W-average-power pump, with 3 W of compressed power with 22 fs pulses [101]. Commercial products based on an ultrafast oscillator and a single, cryogenically cooled regenerative amplifier provide average powers in the 10–12 W range, for pulse rates from 1 to 300 kHz, and pulse widths ≤40 fs [102].

At present, commercial, cryogenically cooled, single multipass amplifier systems produce as much as 5 mJ of compressed energy at 1 kHz and 1 mJ at 10 kHz, for 10 W of average power, with ≤25 fs pulses. Systems with two to three multipass stages generate as much as 20 mJ of energy at 1 kHz and 5 mJ at 10 kHz (50 W of average power), also with ≤25 fs pulses [103]. Similar performance is available from commercial systems combining regenerative and multipass amplifiers, but the pulse widths are specified as ≤40 fs [104].

In lower-pulse-rate, higher-energy systems, a four-pass amplifier, with 200 mJ of input, generated 3.5 J of energy with 9.8 J of 532 nm pump energy, leading to a compressed output of 2.5 J in 25 fs pulses, at a 10 Hz rate [105]. Another system with a 40 mm-diameter crystal and 6.5 J of 532 nm pump energy produced 3.2 J of output energy with a 260 mJ input, also at a 10 Hz rate [106].

REFERENCES

1. T. H. Maiman, "Stimulated optical radiation in ruby," *Nature*, vol. 187, p. 493, 1960.
2. L. F. Johnson, R. E. Dietz, and H. J. Guggenheim, "Optical maser oscillation from N^{2+} in MgF_2, involving simultaneous emission of phonons," *Phys. Rev. Lett*., vol. 11, no. 7, pp. 318–320, Oct. 1963, doi: 10.1103/PhysRevLett.11.318.
3. L. F. Johnson, R. E. Dietz, and H. J. Guggenheim, "Spontaneous and stimulated emission from Co^{2+} ions in MgF_2 and ZnF_2," *Appl. Phys. Lett*., vol. 5, no. 2, pp. 21–22, Jul. 1964, doi: 10.1063/1.1754029.
4. L. F. Johnson, H. J. Guggenheim, and R. A. Thomas, "Phonon-terminated optical masers," *Phys. Rev.*, vol. 149, p. 179, 1966.
5. L. F. Johnson and H. J. Guggenheim, "Phonon terminated coherent emission from V^{2+} ions in MgF_2," *J. App. Phys.*, vol. 38, p. 4837, 1967.
6. P. F. Moulton, "Tunable solid state lasers," *Proc. IEEE*, vol. 80, p. 348, 1992.
7. J. C. Walling, H. P. Jenssen, R. C. Morris, E. W. O'Dell, and O. G. Peterson, "Tunable-laser performance in $BeAl_2O_4$:Cr^{3+}," *Opt. Lett*., vol. 4, no. 6, pp. 182–183, Jun. 1979, doi: 10.1364/OL.4.000182.
8. J. C. Walling, O. G. Petersen, H. P. Jenssen, R. C. Morris, and E. W. O'Dell, "Tunable alexandrite lasers," *IEEE J. Quantum Electron*., vol. 16, p. 1302, 1980.
9. S. A. Payne, L. L. Chase, H. W. Newkirk, L. K. Smith, and W. F. Krupke, "$LiCaAlF_6$:Cr^{3+}: a promising new solid-state laser material," *IEEE J. Quantum Electron*., vol. 24, no. 11, pp. 2243–2252, Nov. 1988, doi: 10.1109/3.8567.
10. S. A. Payne, L. L. Chase, L. K. Smith, W. L. Kway, and H. W. Newkirk, "Laser performance of $LiSrAlF_6$:Cr^{3+}," *J. Appl. Phys*., vol. 66, p. 1051, 1989.
11. W. F. Krupke, "Insulator materials in high power lasers for inertial fusion: present and future," in *MRS Proceedings*, vol. 24, p. 401, Jan. 1983, doi: 10.1557/PROC-24-401.
12. W. F. Krupke, M. D. Shinn, J. E. Marion, J. A. Caird, and S. E. Stokowski, "Spectroscopic, optical, and thermomechanical properties of neodymium- and chromium-doped gadolinium scandium gallium garnet," *J. Opt. Soc. Am*., vol. B3, p. 102, 1986.
13. B. W. Woods, S. A. Payne, J. E. Marion, R. S. Hughes, and L. E. Davis, "Thermomechanical and thermo-optical properties of the $LiCaAlF_6$:Cr^{3+} laser material," *J. Opt. Soc. Am*., vol. B8, p. 970, 1991.
14. S. A. Payne et al., "Properties of Cr:$LiSrAlF_6$ crystals for laser operation," *Appl. Opt*., vol. 33, p. 5526, 1994.
15. R. D. Peterson, A. T. Pham, H. P. Jenssen, A. Cassanho, and V. Castillo, "Thermo-optical comparison of LiSAF, LiCAF, and LiSGaF," in *OSA Trends in Optics and Photonics Vol. 26, Advanced Solid State Lasers*, M. M. Fejer, H. Injeyan, and U. Keller, Eds. Washington, DC: Optical Society of America, 1999, vol. 26, pp. 647–651.
16. M. G. Holland, "Thermal conductivity of several optical laser materials," *J. Appl. Phys*., vol. 33, p. 2910, 1962.

17. P. F. Moulton, "Spectroscopic and laser characteristics of Ti:Al_2O_3," *J. Opt. Soc. Am. B*, vol. 3, p. 125, 1985.
18. R. L. Aggarwal, A. Sanchez, R. E. Fahey, and A. J. Strauss, "Magnetic and optical measurements on Ti:Al_2O_3 crystals for laser applications: concentration and absorption cross section of Ti^{3+} ions," *Appl. Phys. Lett.*, vol. 48, p. 1345, 1986.
19. N. P. Barnes and D. K. Remelius, "Amplifier and line-narrowed oscillator performance of Ti:Al_2O_3," in *Tunable Solid-State Lasers II*, A. B. Budgor, Ed. Berlin Heidelberg: Springer-Verlag, 1986, p. 318.
20. B. C. Stuart, S. Herman, and M. D. Perry, "Chirped-pulse amplification in Ti:sapphire beyond 1 µm," *IEEE J. Quantum Electron.*, vol. 31, p. 528, 1995.
21. K. Ertel, C. Hooker, S. J. Hawkes, B. T. Parry, and J. L. Collier, "ASE suppression in a high energy Titanium sapphire amplifier," *Opt. Exp.*, vol. 16, p. 8039, 2008.
22. E. D. Nelson, J. Y. Wong, and A. L. Schawlow, "Far infrared spectra of Al_2O_3:Cr^3+ and Al_2O_3:Ti^{3+}," *Phys. Rev.*, vol. 156, pp. 298–308, 1967.
23. R. R. Joyce and P. L. Richards, "Far infrared spectra of Al_2O_3 doped with Ti, V and Cr," *Phys. Rev.*, vol. 179, pp. 375–380, 1969.
24. R. M. MacFarlane, J. Y. Wong, and M. D. Sturge, "Dynamic Jahn-Teller effect in octahedrally coordinated d^1 impurity systems," *Phys. Rev.*, vol. 166, pp. 250–258, 1968.
25. I. H. Malitson and M. J. Dodge, "Refractive index and birefringence of synthetic sapphire," *Latter Appears Handb. Opt. Mater.*, vol. 62, p. 1405, 1972.
26. J. F. Pinto, L. Esterowitz, G. H. Rosenblatt, M. Kokta, and D. Peressini, "Improved Ti:sapphire laser performance with new high figure of merit crystals," *IEEE J. Quantum Electron.*, vol. 30, p. 2612, 1994.
27. F. Schmid and C. P. Khattak, "Growth of Co:MgF_2, and Ti:Al_2O_3 crystals for solid state laser applications," in *Tunable Solid State Lasers*, P. Hammerling, A. B. Budgor, and A. Pinto, Eds. New York: Springer, 1985, pp. 122–128.
28. J. Harrison, A. Finch, D. M. Rines, G. A. Rines, and P. F. Moulton, "Low-threshold, cw, all-solid-state Ti:Al_2O_3 laser," *Opt. Lett.*, vol. 16, p. 581, 1999.
29. A. J. Alfrey, "Modeling of longitudinally pumped cw Ti:sapphire laser oscillators," *IEEE J. Quantum Electron.*, vol. 25, p. 760, 1989.
30. H. Kogelnik, P. I. E, A. Dienes, and C. V. Shank, "Astigmatically compensated cavities for cw dye lasers," *IEEE J. Quantum Electron.*, vol. 8, p. 373, 1972.
31. W. D. Johnston and P. K. Runge, "An improved astigmatically compensated resonator for CW dye lasers," *IEEE J. Quantum Electron.*, vol. 8, p. 724, 1972.
32. H. Kogelnik, T. Li, A. Massey, and A. E. Siegman, "Laser beams and resonators," *Appl. Opt.*, vol. 5, p. 1550, 1966.
33. J. Harrison, A. Finch, D. M. Rines, G. A. Rines, and P. F. Moulton, "Low-threshold, cw, all-solid-state Ti:Al_2O_3 laser," *Opt. Lett.*, vol. 16, p. 581, 1991.
34. C. L. Tang, H. Statz, and G. deMars, "Spectral output and spiking behavior of solid-state lasers," *J. Appl. Phys.*, vol. 34, p. 2289, 1963.
35. A. R. Clobes and M. J. Brienza, "Single-frequency traveling-wave Nd:YAG laser," *Appl. Phys. Lett.*, vol. 21, p. 265, 1972.
36. P. A. Schulz, "Single-frequency Ti:Al_2O_3 ring laser," *IEEE J. Quantum Electron.*, vol. 24, p. 1039, 1988.
37. T. F. Johnston, Jr. and W. Proffitt, "Design and performance of a broad-band optical diode to enforce one-direction traveling-wave operation of a ring laser," *IEEE J. Quantum Electron.*, vol. 16, p. 483, 1980.
38. W. Vassen, C. Zimmermann, R. Kallenbach, and T. W. Hansch, "A frequency-stabilized titanium sapphire laser for high-resolution spectroscopy," *Opt. Commun.*, vol. 75, p. 435, 1990.
39. J. M. Yarborough and J. L. Hobart, "Tuning apparatus for an optical oscillator," US Patent 3,934,210. Note that Fig. 4 incorrectly indicates Brewster's angle.
40. U. Demirbas, "Off-surface optic axis birefringent filters for smooth tuning of broadband lasers," *Appl. Opt.*, vol. 56, p. 7815, 2017.
41. D. Bruneau, H. Cazeneuve, C. Loth, and J. Pelon, "Double-pulse dual-wavelength alexandrite laser for atmospheric water vapor measurement," *Appl. Opt.*, vol. 30, p. 3932, 1991.
42. G. Holtom and O. Teschke, "Design of a birefringent filter for high-power dye-lasers," *IEEE J. Quantum Electron.*, vol. 10, p. 577, 1974.
43. I. J. Hodgkinson and J. I. Vukusic, "Birefringent filters for tuning flashlamp-pumped dye lasers: simplified theory and design," *Appl. Opt.*, vol. 17, no. 12, pp. 1944–1948, Jun. 1978, doi: 10.1364/AO.17.001944.
44. S. Lovold, P. F. Moulton, D. K. Killinger, and N. Menyuk, "Frequency tuning characteristics of a Q-switched Co:MgF_2 laser," *IEEE J. Quantum Electron.*, vol. 21, p. 202, 1985.
45. K. Naganuma, G. Lenz, and E. P. Ippen, "Variable bandwidth birefringent filter for tunable femtosecond lasers," *IEEE J. Quantum Electron.*, vol. 28, p. 2142, 1992.
46. S. M. Kobtsev and N. A. Sventsitskay, "Application of birefringent filters in continuous-wave tunable lasers: a review," *Opt. Spectrosc.*, vol. 73, p. 114, 1992.
47. Spectra-Physics Model 3900S Data Sheet SP-DS-20150918. Permission to use granted by MKS/Spectra-Physics. All rights reserved, 2015.
48. P. W. Roth, A. J. Maclean, D. Burns, and A. J. Kemp, "Directly diode-laser-pumped Ti:sapphire laser," *Opt. Lett.*, vol. 34, p. 3334, 2009.
49. P. W. Roth, A. J. Maclean, D. Burns, and A. J. Kemp, "Direct diode-laser pumping of a mode-locked Ti:sapphire laser," *Opt. Lett.*, vol. 36, p. 304, 2011.
50. C. G. Durfee et al., "Direct diode-pumped Kerr-lens mode-locked Ti:sapphire laser," *Opt. Express*, vol. 20, p. 13677, 2012.
51. K. Gürel et al., "Green-diode-pumped femtosecond Ti:sapphire laser with up to 450 mW average power," *Opt. Express*, vol. 23, 30043, 2015.
52. R. Sawada, H. Tanaka, N. Sugiyama, and F. Kannari, "Wavelength-multiplexed pumping with 478- and 520-nm indium gallium nitride laser diodes for Ti:sapphire laser," *Appl. Opt.*, vol. 56, p. 1654, 2017.
53. P. F. Moulton, J. G. Cederberg, K. T. Stevens, G. Foundos, M. Koselja, and J. Preclikova, "Optimized InGaN-diode pumping of Ti:sapphire crystals," *Opt Mater. Express*, vol. 9, pp. 2131–2146, 2019.
54. P. F. Moulton, J. G. Cederberg, K. T. Stevens, G. Foundos, M. Koselja, and J. Preclikova, "Characterization of absorption bands in Ti:sapphire crystals," *Opt. Mater. Express*, vol. 9, pp. 2216–2251, 2019.

55. J.-C. Diels and W. Rudolph, *Ultrashort Laser Pulse Phenomena: Fundamentals, Techniques, and Applications on a Femtosecond Time Scale*. Amsterdam: Elsevier, 2006.
56. L. Dahlström, "Passive mode-locking and Q-switching of high power lasers by means of the optical Kerr effect," *Opt. Commun.*, vol. 5, pp. 157–162, 1972.
57. E. G. Lariontsev and V. N. Serkin, "Possibility of using self-focusing for increasing contrast and narrowing of ultrashort light pulses," *Sov. J. Quantum Electron.*, vol. 5, p. 796, 1975.
58. L. R. Brovelli, "Self-starting soliton modelocked Ti-sapphire laser using a thin semiconductor saturable absorber," *Electron. Lett.*, vol. 31, pp. 287–289, 1995.
59. H. A. Haus, "Mode-locking of lasers," *IEEE J. Sel. Top. Quantum Electron.*, vol. 6, pp. 1173–1185, 2000.
60. P. G. Drazin and R. S. Johnson, *Solitons: An Introduction*. Cambridge: Cambridge University Press, 1989.
61. G. L. Lamb, *Elements of Soliton Theory*. New York: Wiley, 1980.
62. J. Herrmann, "Theory of Kerr-lens mode locking: role of self-focusing and radially varying gain," *JOSA B*, vol. 11, pp. 498–512, 1994.
63. U. Keller, "Semiconductor saturable absorber mirrors (SESAM's) for femtosecond to nanosecond pulse generation in solid-state lasers," *IEEE J. Sel. Top. Quantum Electron.*, vol. 2, pp. 435–453, 1996.
64. F. Gires and P. Tournois, "An interferometer useful for pulse compression of a frequency modulated light pulse," *CR Acad. Sci.*, vol. 258, pp. 6112–6115, 1964.
65. R. L. Fork, O. E. Martinez, and J. P. Gordon, "Negative dispersion using pairs of prisms," *Opt. Lett.*, vol. 9, pp. 150–152, 1984.
66. M. Ramaswamy-Paye and J. G. Fujimoto, "Compact dispersion-compensating geometry for Kerr-lens mode-locked femtosecond lasers," *Opt. Lett.*, vol. 19, pp. 1756–1758, 1994.
67. R. Szipöcs, C. Spielmann, F. Krausz, and K. Ferencz, "Chirped multilayer coatings for broadband dispersion control in femtosecond lasers," *Opt. Lett.*, vol. 19, pp. 201–203, 1994.
68. M. Cervantes, "Brewster angle prisms: a review," *Opt. Laser Technol.*, vol. 20, pp. 297–300, 1988.
69. B. E. Lemoff and C. P. J. Barty, "Cubic-phase-free dispersion compensation in solid-state ultrashort-pulse lasers," *Opt. Lett.*, vol. 18, pp. 57–59, 1993.
70. R. Ell, "Generation of 5-fs pulses and octave-spanning spectra directly from a Ti:sapphire laser," *Opt. Lett.*, vol. 26, pp. 373–375, 2001.
71. R. Holzwarth, "Optical frequency synthesizer for precision spectroscopy," *Phys. Rev. Lett.*, vol. 85, pp. 2264–2267, 2000.
72. D. J. Jones, "Carrier-envelope phase control of femtosecond mode-locked lasers and direct optical frequency synthesis," *Science*, vol. 288, pp. 635–639, 2000.
73. J. L. Hall, "Nobel lecture: defining and measuring optical frequencies," *Rev. Mod. Phys.*, vol. 78, pp. 1279–1295, 2006.
74. T. W. Hänsch, "Nobel lecture: passion for precision," *Rev. Mod. Phys.*, vol. 78, pp. 1297–1309, 2006.
75. J. Ye and S. T. Cundiff, *Femtosecond Optical Frequency Comb: Principle, Operation and Applications*. Boston, MA: Springer Science & Business Media, 2005.
76. R. Holzwarth, M. Zimmermann, T. Udem, and T. W. Hansch, "Optical clockworks and the measurement of laser frequencies with a mode-locked frequency comb," *IEEE J. Quantum Electron.*, vol. 37, pp. 1493–1501, 2001.
77. P. B. Corkum and F. Krausz, "Attosecond science," *Nat. Phys.*, vol. 3, p. 381, 2007.
78. J. Reichert, R. Holzwarth, Th. Udem, and T. W. Hänsch, "Measuring the frequency of light with mode-locked lasers," *Opt. Commun.*, vol. 172, no. 1, pp. 59–68, Dec. 1999, doi: 10.1016/S0030-4018(99)00491-5.
79. F. Lücking, A. Assion, A. Apolonski, F. Krausz, and G. Steinmeyer, "Long-term carrier-envelope-phase-stable few-cycle pulses by use of the feed-forward method," *Opt. Lett.*, vol. 37, pp. 2076–2078, 2012.
80. D. Strickland and G. Mourou, "Compression of amplified chirped optical pulses," *Opt. Commun.*, vol. 56, no. 3, pp. 219–221, Dec. 1985, doi: 10.1016/0030-4018(85)90120-8.
81. P. Maine, D. Strickland, P. Bado, M. Pessot, and G. Mourou, "Generation of ultrahigh peak power pulses by chirped pulse amplification," *IEEE J. Quantum Electron.*, vol. 24, no. 2, pp. 398–403, Feb. 1988, doi: 10.1109/3.137.
82. M. Pessot, J. Squier, G. Mourou, and D. J. Harter, "Chirped-pulse amplification of 100-fs pulses," *Opt. Lett.*, vol. 14, no. 15, pp. 797–799, Aug. 1989, doi: 10.1364/OL.14.000797.
83. S. Backus, C. Durfee, and M. Murnane, "High power ultrafast lasers," *Rev. Sci. Instrum.*, vol. 69, p. 1207, Jun. 1998, doi: 10.1063/1.1148795.
84. J. E. Murray and W. H. Lowdermilk, "Nd:YAG regenerative amplifier," *J. Appl. Phys.*, vol. 51, no. 7, pp. 3548–3556, 1980, doi: 10.1063/1.328194.
85. C. P. J. Barty et al., "Regenerative pulse shaping and amplification of ultrabroadband optical pulses," *Opt. Lett.*, vol. 21, no. 3, pp. 219–221, Feb. 1996, doi: 10.1364/OL.21.000219.
86. C. P. J. Barty et al., "Generation of 18-fs, multiterawatt pulses by regenerative pulse shaping and chirped-pulse amplification," *Opt. Lett.*, vol. 21, no. 9, pp. 668–670, May 1996, doi: 10.1364/OL.21.000668.
87. H. Takada, M. Kakehata, and K. Torizuka, "High-repetition-rate 12fs pulse amplification by a Ti:sapphire regenerative amplifier system," *Opt. Lett.*, vol. 31, no. 8, pp. 1145–1147, Apr. 2006, doi: 10.1364/OL.31.001145.
88. M. P. Minitti et al., "Optical laser systems at the Linac coherent light source," *J. Synchrotron. Radiat.*, vol. 22, no. 3, Art. no. 3, May 2015, doi: 10.1107/S1600577515006244.
89. W. H. Lowdermilk and J. E. Murray, "The multipass amplifier: theory and numerical analysis," *J. Appl. Phys.*, vol. 51, no. 5, pp. 2436–2444, May 1980, doi: 10.1063/1.328014.
90. C. L. Blanc, G. Grillon, J. P. Chambaret, A. Migus, and A. Antonetti, "Compact and efficient multipass Ti:sapphire system for femtosecond chirped-pulse amplification at the terawatt level," *Opt. Lett.*, vol. 18, no. 2, pp. 140–142, Jan. 1993, doi: 10.1364/OL.18.000140.
91. F. Tavella, A. Marcinkevičius, and F. Krausz, "Investigation of the superfluorescence and signal amplification in an ultrabroadband multiterawatt optical parametric chirped pulse amplifier system," *New J. Phys.*, vol. 8, p. 219, 2006.

92. A. Jullien et al., "10^{-10} temporal contrast for femtosecond ultraintense lasers by cross-polarized wave generation," *Opt. Lett.*, vol. 30, p. 920, 2005.
93. V. Chvykov, J. Nees, and K. Krushelnick, "Transverse amplified spontaneous emission: the limiting factor for output energy of ultra-high power lasers," *Opt. Commun.*, vol. 312, p. 216, 2014.
94. Z. Gan et al., "200 J high efficiency Ti:sapphire chirped pulse amplifier pumped by temporal dual-pulse," *Opt. Express*, vol. 25, p. 5169, 2017.
95. D. N. Papadopoulos et al., "The Apollon 10 PW laser: experimental and theoretical investigation of the temporal characteristics," *High Power Laser Sci. Eng.*, vol. 4, p. 34, 2016.
96. R. Dabu, "High power femtosecond lasers at ELI-NP," in *AIP Conference Proceedings* vol. 1645, p. 219., 2015, doi: 10.1063/1.4909578.
97. F. Lureau et al., "Latest results of 10 petawatt laser beamline for ELi nuclear physics infrastructure," *Proc. SPIE*, vol. 9726, p. 972613, 2016.
98. National Academies of Sciences, Engineering, and Medicine. *Opportunities in Intense Ultrafast Lasers: Reaching for the Brightest Light*. Washington, DC: The National Academies Press, 2017.
99. P. A. Schulz and S. R. Henion, "Liquid-nitrogen-cooled Ti:Al_2O_3 laser," *IEEE J. Quantum Electron.*, vol. 27, p. 1139, 1991.
100. I. Matsushima, H. Yashiro, and T. Tomie, "10 kHz 40W Ti:sapphire regenerative ring amplifier," *Opt. Lett.*, vol. 31, p. 2066, 2006.
101. J. H. Sung, H. W. Lee, C. H. Nam, and S. K. Lee, "100-kHz 22-fs Ti:sapphire regenerative amplification laser with programmable spectral control," *Appl. Phys. B*, vol. 122, p. 125, 2016.
102. KMLabs, *Wyvern Product Line*. Boulder, CO: KMLabs.
103. KMLabs, *Dragon and Red-Dragon Product Lines*. Boulder, CO: KMLabs.
104. KMLabs, *Red-Wyvern Product Lines*. Boulder, CO: KMLabs.
105. M. Pittman, S. Ferré, J. P. Rousseau, L. Notebaert, J. P. Chambaret, and G. Chériaux, "Design and characterization of a near-diffraction-limited femtosecond 100-TW 10-Hz high-intensity laser system," *Appl. Phys. B*, vol. 74, no. 6, pp. 529–535, Apr. 2002, doi: 10.1007/s003400200838.
106. H. Kiriyama et al., "High temporal and spatial quality petawatt-class Ti:sapphire chirped-pulse amplification laser system," *Opt. Lett.*, vol. 35, p. 1497, 2010.